Numerical Study on Tone Noise of Different Thickness Airfoils

IOP Conf. Series: Materials Science and Engineering **538** (2019) 012052 doi:10.1088/1757-899X/538/1/012052

Numerical Study on Tone Noise of Different Thickness Airfoils

Feng Huanhuan, Liu Yong[a], Wang Qi and Zou Sen

Nanchang Hang Kong University, School of Aircraft Engineering, 330063 Nanchang Jiangxi, China

[a]Corresponding author: liuyong@nchu.edu.cn

Abstract. Based on the Lattice Boltzmann Method(LBM)-Large Eddy Simulation(LES), a direct numerical calculation is presented of tone noise generated by flow past symmetric NACA airfoils with different thickness and at a Reynolds number based on chord of $\mathrm{Re} = 2.0 \times 10^5$. The computation results indicate that the acoustic source of the airfoil mainly at region of trailing edge and the flow separation. For NACA series airfoils with different thicknesses of the same curvature, the increase of thickness could enlarge pressure fluctuation and produce larger scale of vortices. Noise sources are identified in the region of trailing edge and the flow separation. The sound pressure level spectrum analysis shows that the tone noise gradually disappears and the noise spectrum displays broadband features with the increases of airfoil thickness. The noise directivity shows that the sound pressure radiation around the airfoil characteristic the dipole acoustic field. In addition, data analysis shows that the generation of tone noise is closely related to the vortex shedding of the trailing edge of the airfoil.

1. Introduction

With the wide application of small or micro unmanned aerial vehicles, wind turbines and etal, the problem of airfoil flow around middle and low Reynolds number （$10^4 < \mathrm{Re} < 10^6$）has received extensive attention in many military and civil flight engineering applications[1-2]. At these operating conditions, laminar boundary layer transition may occur on the airfoil due to an adverse pressure gradient, which may cause strong tone noise or broadband noise[3]. The increasingly serious noise problem, especially aerodynamic noise of rotating machinery and aircraft has gradually become an important factor affecting human health. Therefore, the research on the problem of airfoil tone noise is of great significance for engineering application problems such as low noise design of related mechanical equipment.

In recent years, many scholars have conducted a lot of repeated research on airfoil tone noise. Arbey & Bataille [4] conducted an experimental study on the noise generated by the NACA0012 airfoil in uniform laminar flow. It is believed that the generation of discrete tone noise at the trailing edge be ascribed to the scattering of instability waves, originating upstream and amplited through the separated shear layer, at the trailing edge. Atassi [5] found that the existence of boundary separation upstream of the trailing edge indicates that the Kelvin-Helmholtz instability as the cause for disturbance amplification. The resulting strong vortical structures convect past the trailing edge at a shedding frequency f_{sh} equal to that of the primary frequency $f_{n_{\max}}$. S. Pröbsting & S. Yarusevych [6] studied

the feedback effect of tone noise generated by the airfoil suction surface separation bubble by PIV technique at the low Reynolds number. The results show that disturbance amplification on the suction and pressure surfaces causing roll-up vortices in separation bubbles and separated shear layers. When the vortex do not rupture upstream of the trailing edge, the passage of these structures over the trailing edge generates tonal noise. Huang Qian of Tsinghua University [7] used the large eddy simulation method to carry out the numerical simulation of the serrated trailing edge airfoil based on the NACA0018 airfoil. It was found that the airfoil pure tone noise is closely related to the state near the trailing edge, but did not make further studies.

Although some research has been done on tone noise of airfoils, many problems remain unclear due to the complexity of the process, especially the influence of airfoil geometry on tone noise. Therefore, the numerical calculations are conducted of NACA0008, NACA0012, NACA0015 and NACA0018 airfoils at zero incidence. The influence of airfoil thickness on tone noise was studied and research results have important reference significance for future low noise airfoil design.

2. Numerical Method

2.1. LBM

The Multiple-Relaxation Time (MRT) lattice Boltzmann equation (1) is given in discrete formulation in momentum space as:

$$\left|f_\alpha(x_i + e_\alpha\delta t, t + \delta t)\right\rangle - \left|f_\alpha(x_i, t)\right\rangle = M^{-1}\hat{S}\left[\left|m(x,t)\right\rangle - \left|m^{(eq)}(x_i,t)\right\rangle\right] \quad (1)$$

where δt is the time step; $\{f_\alpha|\alpha = 0,1,\ldots,N\}$ is the discretized distribution functions (DFs), which represents the probability to meet a particle at the position at the position x_i at the time t; $\{e_\alpha|\alpha = 0,1,\ldots,N\}$ is the discrete velocities, the superscript *eq* represents the equilibrium state; M is the transformation matrix; $\hat{S}$ is the diagonal relaxation matrix, $m = M \bullet f$ [8].

The discrete velocity model D2Q9[9] is used for the two-dimensional, low Mach number flow. The discrete velocities are given by:

$$e_\alpha = \begin{cases} (0,0) & \alpha = 0 \\ (\cos\theta_\alpha, \sin\theta_\alpha)c & \theta_\alpha = \dfrac{(\alpha-1)\pi}{2} \quad \alpha = 1,2,3,4 \\ \sqrt{2}(\cos\theta_\alpha, \sin\theta_\alpha)c & \theta_\alpha = \dfrac{(\alpha-5)\pi}{2} + \dfrac{\pi}{4} \quad \alpha = 5,6,7,8 \end{cases} \quad (2)$$

Where c is lattice velocity; the velocity distribution function for equilibrium particles is defined as:

$$f_\alpha^{(eq)} = \rho\omega_\alpha\left[1 + \frac{(e_\alpha \cdot u)^2}{c_s^4} - \frac{u^2}{2c_s^2}\right] \quad (3)$$

where c_s is the sound speed; ω_α is the weight parameters, $\omega_0 = \frac{4}{9}$, $\omega_{\alpha=1,2,3,4} = \frac{1}{9}$, $\omega_{\alpha=5,6,7,8} = \frac{1}{36}$; ρ is macroscopic density and u is macroscopic velocity. The macroscopic physical quantities can be obtained by the DFs: $\rho = \sum_{\alpha=0}^{8} f_\alpha$, $\rho u = \sum_{\alpha=0}^{8} f_\alpha e_\alpha$, $p = \rho c_s^2$. Assumping that the Knudsen number and Mach number are small enough, the continuum Navier-Stokes equation would be recovered by the Chapman–Enskog expansion.

For the D2Q9 model, the values of M, m, and m^{eq} can be found in[10]. The diagonal collision matrix $\hat{S}$ can be obtained by the linearization analysis：

$$\hat{S} = \mathrm{diag}(1.0,1.4,1.4,1.0,1.2,1.0,1.2,s_7,s_8) \quad (4)$$

where S_i is collision frequency, and $S_7 = S_8$. The relaxation factors $\tau_i = \frac{1}{S_i}$. The shear viscosity υ can be expressed as:

$$\upsilon = \frac{1}{3}(\tau_7 - \frac{1}{2}) = \frac{1}{3}(\frac{1}{s_7} - \frac{1}{2}), \zeta = \frac{1}{3}(\frac{1}{s_1} - \frac{1}{2}) \tag{5}$$

2.2. LES

The large eddy simulation method assumes that the small scale vortices of the flow below the subgrid scale are similar and isotropic, and thus the subgrid scale model can be used to simulate the effects of the small scale on the large-scale vortices. The eddy viscosity model is the most widely used model for LES. It is only necessary to introduce the eddy viscosity υ_t into the Lattice Boltzmann equation(LBE), without changing the structure of LBE and the algorithm for solving LBE. The eddy viscosity υ_t can be expressed as:

$$\upsilon_t = C_x \Delta^2 |S| \tag{6}$$

where C_x is subgrid model constant; Δ is the grid filter width, which is proportional to the grid size; $|S| = \sqrt{2S_{ij}S_{ij}}$, $S_{ij} = \frac{1}{2}(\partial_i u_j + \partial_j u_i)$; S_{ij} can be obtained directly from m in moment space of the MRT-LBM method. However, in the process of solving N-S equations based on finite difference methods, etc, S_{ij} needs to be obtained by calculating the derivative of the physical quantities of adjacent points. The method of solution to S_{ij} is also one of the advantages of applying the LES method to the LB equation.

In the standard subgrid model, C_x is a constant. The dynamic subgrid model C_x can be obtained by filtering twice on a grid of different scales and then by the least squares method [11]. After obtaining the dynamic eddy viscosity υ_t, it is added to the fluid shear viscosity υ, ie $\upsilon = \upsilon_0 + \upsilon_t$, υ_0 is the hydrodynamic viscosity, and then the diagonal collision matrix $\hat{\mathbf{S}}$ can be determined according to the formula (5).

3. Grid and Acoustics Field Monitoring Point

3.1. Grid Design

The computational domain occupies a $40c \times 40c$ square, where c is airfoil chord. Duo to the multi-scale problem for flow over airfoil, it is not suitable using uniform meshes. The non-uniform quadtree grids with high retrieval efficiency is used to improve computation efficiency in this paper. The mesh in computational domain was shown in Fig.1, where the size of mesh is $5.2e^{-4}c$ near the wall and wake. The number of cell was 17 million, and the maximum of Δx^+ is 50 to ensure that the magnitude of the wall maximum Δy^+ [12]. Therefore, the wall function is not needed in the near wall area of the airfoil, and wall-resolved LES was used.

Acoustic applications are highly sensible to reflections of pressure waves that may occur at the inlet and outlet boundary conditions in compressible unsteady simulations. These reflections may interfere with the pressure measurements. To overcome this issue, the non reflecting Dirichlet boundary condition of velocity and pressure is derived from the local one-dimensional Viscous Free (LODI) equation[13]. Therefore, the inlet boundary is set as a velocity condition and the outlet boundary as a Non-reflective boundary condition. The top and bottom boundaries are set as periodic pairs.

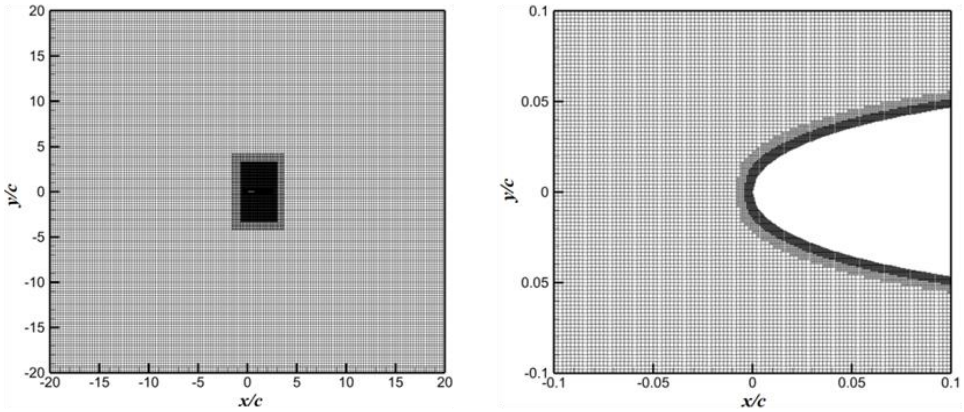

(a) whole domain (b) Grid details around airfoil leading edge

Figure 1. Grid in computational domain

3.2. Acoustic Field Monitoring Point Setup

The LBM-LES method can directly obtain the density fluctuation $\rho`$ of the fluid. The pressure fluctuation is similar to the sound pressure fluctuation far from the airfoil, and according to the formula $p = \rho c_s^2$ ($c_s$ is a constant), so the pressure fluctuation of the fluid is obtained $p` = \rho` c_s^2$, and the pressure fluctuation of the flow field and the sound field can be obtained by the formula[14]. Four monitoring points are placed vertically above and below the trailing edge of the airfoil from the trailing edge 0.5c and 1c, respectively. In addition, with the airfoil leading edge point as the center, 24 monitoring points are uniformly set in the near field of radius $r = 5c$ and the far field of $r = 10c$ as shown in figure 2:

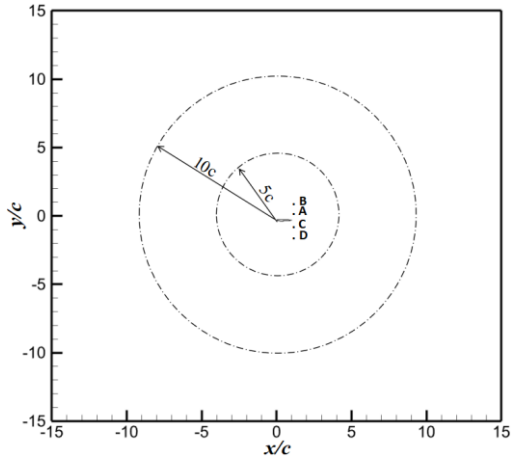

Figure 2. Acoustic field monitoring point distribution

4. Results and Discussion

In order to verify the reliability of the numerical method in this paper, the numerical calculations are performed of NACA0012 airfoil at 2° angle of attack and a Reynolds number based on chord of $\mathrm{Re} = 2.0 \times 10^5$. And the calculation results of aerodynamic and noise performance are compared with the reference values in the literature [15-16]. It can be seen from Fig. 3 that the mean pressure coefficient distribution obtained by LBM-LES method agrees well with the experimental values of Mckee[15]. At the same time, it can be seen from Fig.4 that the sound pressure level spectrum of the monitoring point A obtained by LBM-LES method shows obvious spectral characteristics of tone noise, which is in

good agreement with the trend of the results obtained by Desquesnes[16] using the DNS method and the maximum peak value of the sound pressure level is basically the same.

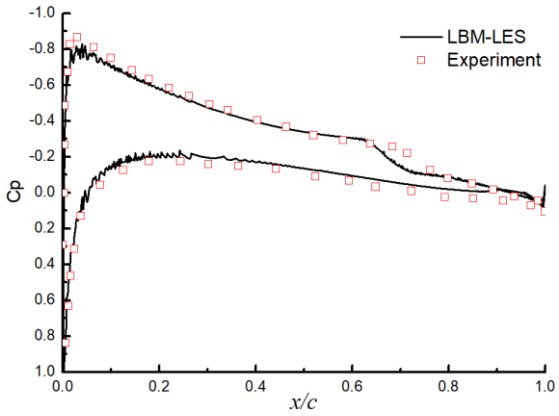

Figure 3. Mean pressure distribution on airfoil surface

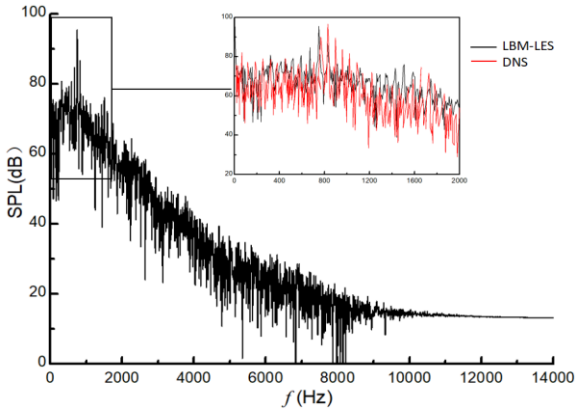

Figure 4. Sound pressure level spectra on point A

The aerodynamic performance and noise characteristics of four different thickness airfoils NACA0008, NACA0012, NACA0015 and NACA0018 were directly calculated by LBM-LES method at 0° angle of attack. The free stream Mach number is 0.1 and the Reynolds number based on chord was specified as $\mathrm{Re}=2.0\times10^{5}$.

Figure 5 shows the instantaneous vorticity and streamline for different thickness airfoils. For small thickness airfoils, the flow is mainly attached and there is no apparent vortex shedding is detected at the trailing edge of the airfoil. The local high curvature produces strong adverse pressure gradient with the increase of airfoil thickness, laminar boundary layer separation may occur on both the upper and lower surfaces of the airfoil. The free shear layer rolls up duo to Kelvin - Helmholtz instability and forms vortex structure. As for the thicker airfoil, more complex separation flow and vortex splitting and merging will be accompanied, resulting in a larger scale vortex structure, and the vortex structure will become more complex and strong.

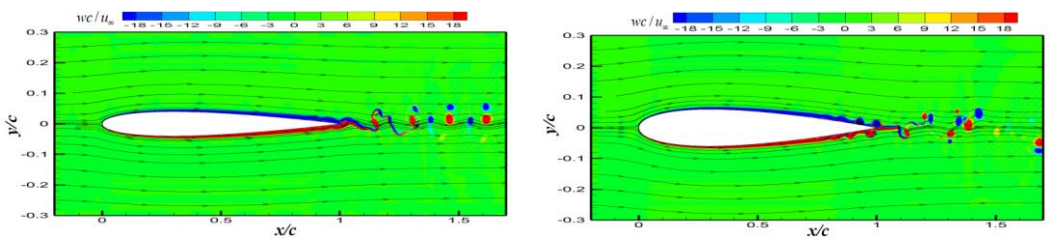

(a) NACA0008 (b) NACA0012

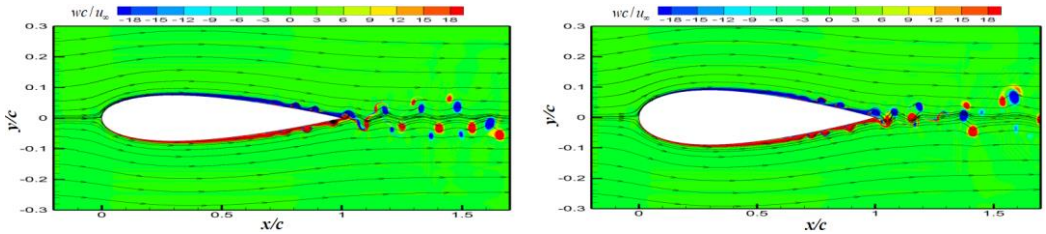

(c) NACA0015 (d) NACA0018

Figure 5. Instantaneous vorticity and streamline contours for different thickness airfoil

Figure 6 visualizes the near-field RMS pressure fluctuation for different thickness airfoils. The root mean squared pressure fluctuations p_{rms} is somewhat considered as a measure of the strength of sound sources. In this paper, p_{rms} is therefore defined by the following way:

$$p_{rms} = \sqrt{(\int_0^T (p - \overline{p})^2 dt / T}$$

Where, p denotes the instantaneous pressure and $\overline{p}$ is the time-averaged pressure. At 0° angle of attack, the RMS pressure distribution is symmetric about the centerline of the wake, and the main source is located in the trailing edge and wake of the airfoil, which corresponds well to the vorticity and streamline contours. This observation indicates that the region of trailing edge and the separation generation represent major sources of sound [17]. With the increase of airfoil thickness, the values of contour levels are also increased indicating that the sound sources are strengthened. For smaller thickness airfoils, the red area at the trailing edge of the NACA0008 airfoil is not obvious. For larger thickness airfoils, a large red area appears on the lower edge of the NACA0018 airfoil. This indicates that with the thickness of the airfoil increases, the pressure fluctuation at the trailing edge of the airfoil and turbulence intensity gradually increases. According to the definition of the root mean square, it is known that aerodynamic noise increases with the increase of airfoil thickness.

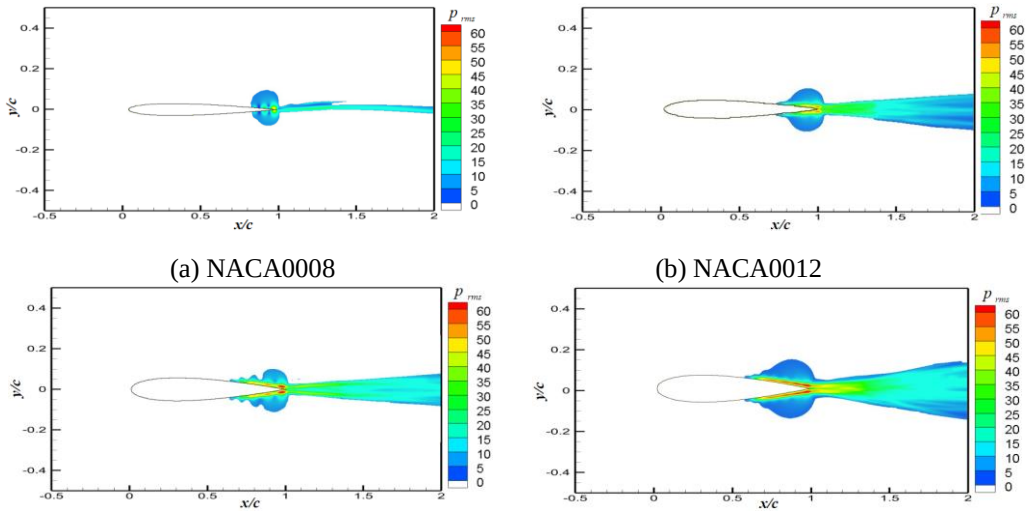

(a) NACA0008 (b) NACA0012

(c) NACA0015 (d) NACA0018

Figure 6. RMS Pressure contours for different thickness airfoil

Figure 7 shows the sound pressure level spectrum on point A for different thickness airfoil. It can be seen from Fig.7 that the first three airfoil sound pressure level spectrums shows obvious spectral characteristics of tone noise at low frequencies, the noise is observed to contain a superposition of discrete tones on a broadband hump [4]. And the spectrum tends to broadband features with the

frequency increases. For the small-thickness airfoil (such as the NACA0008 airfoil), the feature of tone noise spectrum is significantly higher than that of the medium-thickness airfoil (such as NACA0012). For thicker airfoils (such as the NACA0018 airfoil), there is no obvious primary frequency and sound pressure level peak at low frequency, the high frequency band also shows broadband features. With the thickness of the airfoil increases, the turbulence intensity gradually becomes stronger and produce larger scale of vortices. For larger thickness airfoils, the discrete noise will gradually disappear, and the noise spectrum reflects the feature of broadband noise. This is because the appearance of noise is accompanied by the separation and reattachment of the fluid. As the thickness increases, the fluid flow around the airfoil exhibits a high degree of instability, multi-scale vortex structures are produced in the separation and the trailing edges. The combination and splitting of these different scale vortex structures causes the noise to exhibit broadband features. Comparing the sound pressure level spectrum of different thickness airfoils, it can be known that with the thickness of the airfoil increases, the primary frequency $f_{n_{\max}}$ also changes greatly. The frequency of the primary frequency $f_{n_{\max}}$ is 619 Hz, 813 Hz, 649 Hz, respectively. And the spectral characteristics show a tendency to change from discrete to broadband features.

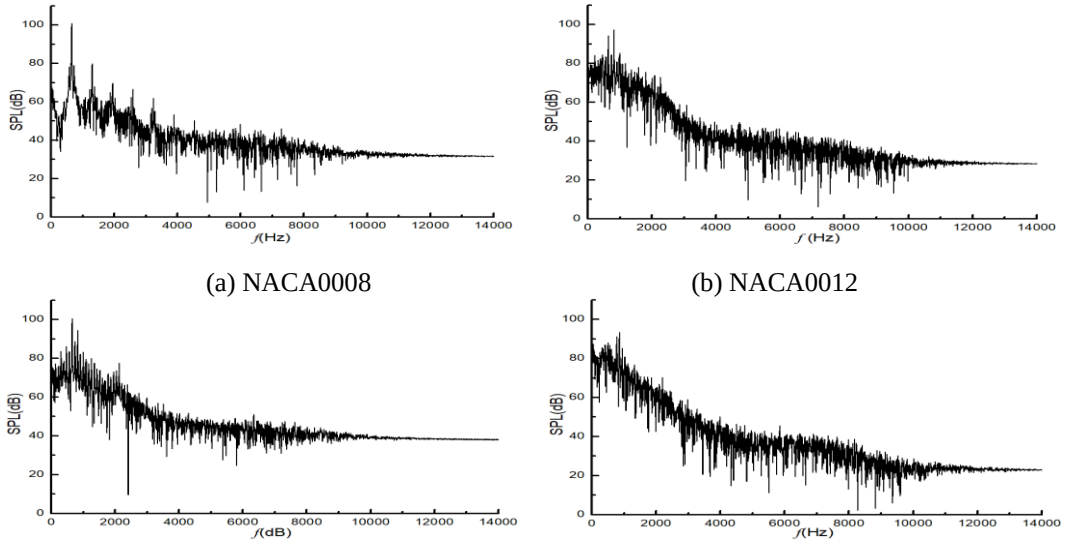

(a) NACA0008 (b) NACA0012

(c) NACA0015 (d) NACA0018

Figure 7. Sound pressure level spectra on point A

Table 1 displays the total sound pressure levels of the four monitoring points. From this table, it can be conclude that the sound pressure level at the monitoring point A is higher than point B, and the sound pressure level at the monitoring point C is higher than point D. This indicates that the sound pressure level on the side of the suction surface is higher than that on the pressure side, but the difference is small. Meanwhile, it can be seen from the table that the sound pressure level increases with the thickness of the airfoil increases.

Table 1. Overall sound pressure level of 4 monitoring points

OASPL（dB）	NACA0008	NACA0012	NACA0015	NACA0018
A	78.2300	91.2709	92.9143	95.1686
B	77.9846	91.2201	92.7415	94.7964
C	75.9843	88.2316	89.7241	91.8628
D	75.6565	88.1651	89.4132	91.5371

The comparison of primary frequency $f_{n_{\max}}$ and vortex shedding frequency f_{sh} on point A are shown in Table 2. From this table, it can be conclude that primary frequency $f_{n_{\max}}$ is closely match the shedding frequency f_{sh}. This indicated that as for the condition of smaller airfoil thickness, vortex shedding at the trailing edge is one of the main factors causing pure tone noise. For larger thickness airfoils (such as NACA0018), the low frequency noise exhibits discrete features, but there is no obvious peak. After 3000Hz, noise spectrum displays broadband features. The main feature of broadband is that the energy at the high frequency position is similar, wide bandwidth and the amplitude is basically within a fixed range.

Table 2. Comparison of primary frequency and vortex shedding frequency on point A

	NACA0008	NACA0012	NACA0015	NACA0018
f_{sh}	619	813	649	_____
$f_{n_{\max}}$	612	802	641	_____

Figure 8 shows the airfoil directivity of OASPL for different thickness airfoil. It can be clearly seen from Fig. 8 that the sound pressure level around the airfoil increases rapidly with the thickness of the airfoil increases. The sound pressure level of the thicker airfoil is 8~12 dB higher than thinner thickness. The sound pressure distribution of the airfoil in the near and far fields is symmetrical. In addition, sound pressure radiation around the airfoil characteristic the dipole acoustic field.

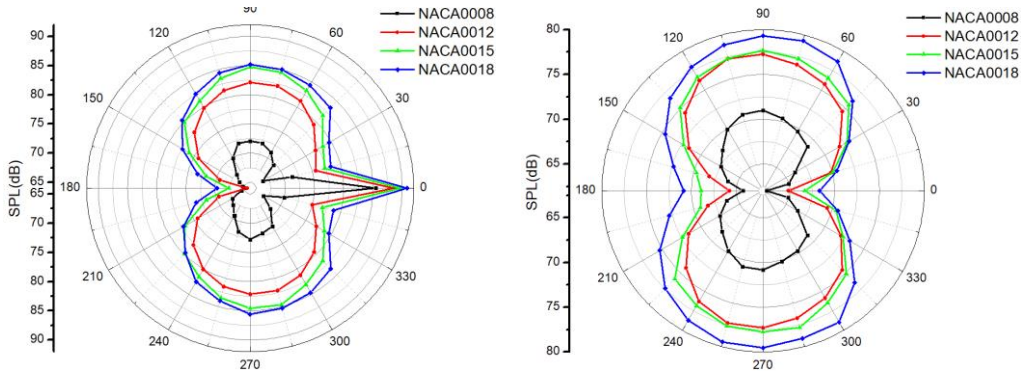

(a) near field (b) far field

Figure 8. Airfoil directivity of OASPL for different thickness airfoil

5. Conclusion

In this paper, based on the LBM-LES method, the direct numerical calculation of four different thickness airfoil tone noise at low and medium Reynolds numbers is performed. The effects of airfoil thickness on tone noise are studied. The conclusion is as follows:

1. The aerodynamic performance and noise characteristics obtained by numerical simulation of the NACA0012 airfoil are in good agreement with the reference literature to verify the reliability of the LBM-LES method.
2. The RMS pressure contours shows that the main sound source of the airfoil mainly at region of trailing edge and the flow separation. The noise directivity shows that the sound pressure radiation around the airfoil characteristic the dipole acoustic field.
3. For NACA series airfoils with different thicknesses of the same curvature, the increase of thickness could enlarge pressure fluctuation and produce larger scale of vortices. The sound pressure level spectrum analysis shows that the tone noise gradually disappears and the noise spectrum displays broadband features with the increases of airfoil thickness. In addition, data analysis shows that the generation of tone noise is closely related to the vortex shedding of the trailing edge of the airfoil.

Acknowledgment
This work was financially supported by project founded by the Science and Technology Research Project of Jiangxi Education Department (GJJ180511), Jiangxi Province Graduate Innovation Fund Project (No. YC2017-S332).

References

[1] Selig M S, Guglielmo J J, "High-Lift Low Reynolds Number Airfoil Design", *Journal of Aircraft*, 34(1):72-79, (1997).
[2] Mutilin J C, Pauley L L, "Low-Reynolds-number separation on an airfoil", *AIAA J*, 34(8): 1570-1577, (1996).
[3] Amiet R K, "Noise due to turbulent flow past a trailing edge", *Journal of Sound & Vibration*, 47(3):387-393,(1976).
[4] Arbey H, Bataille J, "Noise generated by airfoil profiles placed in a uniform laminar flow", *Journal of Fluid Mechanics*, 134(134):33-47, (2006).
[5] Atassi H, "Feedback in separated flows over symmetric airfoils", *Aiaa Journal*, (1984).
[6] Probsting S, Yarusevych S, "Laminar separation bubble development on an airfoil emitting tonal noise", Journal of Fluid Mechanics, 780:167-191, (2015).
[7] Huang Qian, "A Numerical study of flow around airfoil with serrated trailing edges and the aerodynamic noise based on large eddy simulation [D]. Tsinghua University, (2015).
[8] D. d'Humi`eres, I Ginzburg, M. Krafczyk, et al, "Multiple Relaxation Time Lattice Boltzmann Models in Three Dimensions", Phil. Trans. R. Soc, 360:437-451,(2002).
[9] He Yaling, Wang Yong, Li Qing, "Theory and Application of Lattice Boltzmann Method", Science Press, (2009).
[10] Girimaji S, "Lattice Boltzmann Method: Fundamentals and Engineering Applications with Computer Codes", *Aiaa Journal*, 51(4):398–404, (2013).
[11] Georgiadis N J, Rizzetta DP, Fureby C, "Large-Eddy Simulation: current capabilities, recommended practices, and future research," *AIAA J*, 48(8):1772-1784, (2010).
[12] Chen Li, "Study of the methods of the numerical prediction of underwater flow noise based on the lattice Boltzmann method",Wuhan: Huazhong University of Science & Technology, 60-70, (2013).
[13] Brionnaud R, et al, "Direct Noise Computation with a Lattice-Boltzmann Method and Application to Industrial Test Cases", Aiaa/ceas Aeroacoustics Conference, (2015).
[14] Sandberg R D, Jones L E, Sandham N D, et al, "Direct numerical simulations of tonal noise generated by laminar flow past airfoils", *Journal of Sound & Vibration*, 320(4):838-858,(2009).
[15] Mckee M W, "An exploratory investigation of airfoil sections in low Reynolds number subsonic compressible flows", (1998).
[16] Desquesnes G, Terracol M, Sagaut P, "Numerical investigation of the tone noise mechanism over laminar airfoils," *Journal of Fluid Mechanics*, 591:155-182, (2007).
[17] Jiang M, Li X, Lin D, "Numerical Simulation on the Airfoil Self-Noise at Low Mach Number Flows", Aiaa Aerospace Sciences Meeting Including the New Horizons Forum and Aerospace Exposition, 28-39, (2013).
[18] Arcondoulis E J G, Doolan C J, Zander A C, "Airfoil noise measurements at various angles of attack and low Reynolds number", *Schools & Disciplines*, 1-8, (2009).